Insights on the Whirl-Flutter Phenomena of Advanced Turboprops and Propfans

Fred Nitzsche*
Empresa Brasileira de Aeronáutica, São José dos Campos, Brazil

The new aircraft configurations that have two pusher propellers or propfans located at the rear fuselage are susceptible to a whirl-flutter-related instability characterized by a complex dynamic coupling involving not only the propeller-nacelle whirl modes but also the natural modes of the supporting backup structure. It is shown that the single-engine classical whirl-flutter formulation does not correctly predict these particular situations of instability, which were called whirl induced flutter. The problem is treated in this paper in the form of a parametric study using a 15-degree-of-freedom model. The main stiffness properties of both the supporting backup structure and the engine mounting system are systematically changed and the mechanism of the aforementioned phenomenon is explained on simple physical grounds.

Nomenclature

a	= distance between fuselage and propeller centerlines
b	= engine-propeller center-of-mass distance from the pylon elastic axis
d	= propeller distance from the pylon elastic axis
h	= pylon elastic axis flatwise displacement
h_y, h_z	= aft fuselage displacements in the lateral and vertical directions, respectively
I_{p_e}, I_{t_e}	= engine polar and transverse moments of inertia, respectively
I_{p_h}	= propeller polar moment of inertia
I_{x_o}	= aft fuselage polar moment of inertia
I_{x_o}, I_{y_o}	= nacelle polar and transverse moments of inertia, respectively
J/π	= $V/\Omega R$
k_v, k_w	= shock mount system lateral and vertical stiffnesses relative to the nacelle, respectively
k_y, k_z, k_θ	= aft fuselage lateral, vertical, and torsional stiffnesses, respectively
k_α	= k_ψ/k_ϕ
k_δ, k_γ	= pylon flatwise and torsional stiffnesses, respectively
k_ψ, k_ϕ	= shock mount system pitch and yaw stiffnesses relative to the nacelle, respectively
M_o	= aft fuselage mass
m_o, m_e, m_h	= nacelle, engine, and propeller masses, respectively
R	= propeller radius
V	= undisturbed airspeed
v, w	= lateral and vertical displacements of the engine-propeller center of mass with respect to the nacelle, respectively
γ	= pylon rotation about the elastic axis
ζ	= aeroelastic mode damping
θ	= aft fuselage rotation about the aircraft centerline
μ	= dimensionless aerodynamic mass ratio
ϕ, ψ	= pitch and yaw displacements of the engine-propeller rigid body with respect to the nacelle, respectively
Ω	= propeller frequency
ω	= natural frequency, aeroelastic mode frequency

Subscripts

c	= critical value (whirl-flutter condition)
1,2	= relative to power plants 1 and 2

Superscripts

-	= dimensionless parameter
·	= time differentiation

Presented as Paper 89-1235 at the AIAA/ASME/ASCE/AHS/ASC 30th Structures, Structural Dynamics, and Materials Conference, Mobile, AL, April 3-5, 1989; received May 1, 1989; revision received July 27, 1990; accepted for publication Aug. 29, 1990.

*Senior Engineer, Aeronautical Engineering Division; currently Visiting Professor, Instituto Tecnológico de Aeronáutica, Centro Técnico Aeroespacial, 12225 São José dos Campos, Brazil. Member AIAA.

Introduction

IN 1938, Taylor and Browne[1] recognized for the first time the whirl-flutter phenomenon as an aeroelastic instability associated with an elastically supported engine-propeller installation. Since the conditions necessary for the occurrence of the phenomenon could not be fulfilled with the existing technology, its importance remained academic until the 1960s when two flight accidents were reported. After a careful analysis conducted in wind tunnels, it was concluded that these accidents could be attributed to whirl flutter if a sudden reduction in the engine mounting system stiffness properties had occurred in flight.[2] In addition to the experimental investigations, some theoretical parametric studies were performed with the same objective.[3-6] Reed and Bland[3] pioneered the modern whirl-flutter analyses with a detailed study considering a two-degree-of-freedom dynamic model and the aerodynamic theory developed for propellers by Ribner.[7] Also, Houbolt and Reed[4] used a similar approach, but developed their own aerodynamics based on the blade element theory. Bland and Bennett[6] conducted a series of parametric investigations in the wind tunnel to validate the existing theoretical calculations. In this study, both rigid and dynamically scaled experimental models were employed to obtain the propeller coefficients derived independently by Ribner[7] and Houbolt and Reed[4] and the whirl-flutter stability boundaries predicted by the theory. These investigations confirmed that the mathematical models were conservative, but could reproduce the trends observed with the experimental models. Later, Zwaan and Bergh,[8] Bennett and Bland,[9] and Head[10] concluded that the effect of the flexibility of the wing on the whirl-flutter margins would be beneficial. However, only single engine-propeller systems were studied in these works. Ravera[11] developed a theoretical formulation to account for

the effects of the thrust in the whirl-flutter stability and concluded that for the high speeds of interest such influence could be neglected. Baker et al.[12] described the basic mechanism of the whirl-flutter phenomenon and discussed the essential degrees of freedom that needed to be included in the original two-degree-of-freedom idealization to perform a reliable analysis. In fact, the simple two-degree-of-freedom model fails to predict correctly the whirl-flutter onset in complex engine installations when the center of mass is moving with respect to the suspension elastic center. In all of these cases, the two fundamental natural modes necessary to describe the whirl-flutter phenomenon (pitch and yaw) are highly coupled with the lateral and the vertical natural modes of the engine-propeller rigid body. Nevertheless, the basic dynamic mechanism involving the backward and forward whirl modes generated by the action of the propeller gyroscopic forces on the primitive pitch and yaw modes of the mass-spring system remained valid: it was reviewed so that coupled modes involving the center-of-mass motion could be introduced in the analysis.

All of the aforementioned studies were restricted to rigid blades. Although this hypothesis may still be fully supported in conventional propeller-driven aircrafts, V/STOL designs often incorporated flexible or articulated blades. Richardson and Naylor[13] and Reed and Bennett[14] investigated the effect of hinged blades that allow for their out-of-plane motion with respect to the propeller disk. The influence of the modes associated with the blade in-plane flexibility was studied by Richardson et al.[15] in parallel with the ground resonance phenomenon, which is well known in helicopter dynamics. Johnson[16] presented a comprehensive work on the aeroelastic behavior of the tilting proprotors, including the bending-torsion degrees of freedom of both the rotor blades and the wing that supports the proprotor. This work indicates that an accurate representation of the dynamic degrees of freedom of the system is required for a correct prediction of all possible instabilities associated with the operation of complex proprotor configurations.

Advanced Turboprop Configuration

The problem of whirl flutter applied to the new configurations of aircraft, in which two pusher propellers or propfans attached to the aft fuselage cone are employed, was first investigated in a previous paper.[17] Dynamic coupling between the two engines through the flexible backup structure that supports them was observed in a 15-degree-of-freedom mathematical model. This model included not only the well-known important degrees of freedom of the engine-propeller installation relative to the nacelle, but also some additional degrees of freedom that were anticipated to play a fundamental role in the aeroelastic problem, namely, bending and torsion of the two pylons that support the engines, fuselage bending in the vertical and horizontal directions, and fuselage torsion about the aircraft centerline (Fig. 1).

Initial studies on this problem have indicated that, for a characteristic range of stiffness ratios between the engine mounting system and the backup structure (i.e., the pylons and the fuselage cone), a novel type of whirl-flutter-related dynamic instability was observed. The phenomenon was called backup structure propeller whirl-induced flutter or, simply, whirl-induced flutter in Ref. 17. It is characterized by critical modes that are derived from the primitive modes of the backup structure instead of the classical whirl modes involving only the engine-propeller motion relative to the nacelle. For these modes, the largest amplitude of the corresponding eigenvector is associated with a dependent variable that defines a backup structure displacement.

Constructive limitations due to the maximum allowable displacement of the engine relative to the nacelle necessarily direct the engine suspension system designer to adopt relatively high values of spring rates for the shock mounts. This leads to a design in which the engine suspension is as stiff as the backup structure itself. As a result, the backup structure modes are highly coupled with the propeller whirl modes and a case of whirl-induced flutter is likely to occur.

Parametric studies with the model just defined were first performed in Ref. 17. Some of the conclusions that could be readily drawn are as follows:

1) The pusher installation is more stable than the tractor and, as expected, it is not susceptible to the static instability (divergence).

2) Counter-rotating propellers lead to larger stability margins.

3) The backup structure influence on the whirl-flutter stability is paramount. It may act as a dynamic damper in many situations, enlarging the stability boundaries in agreement

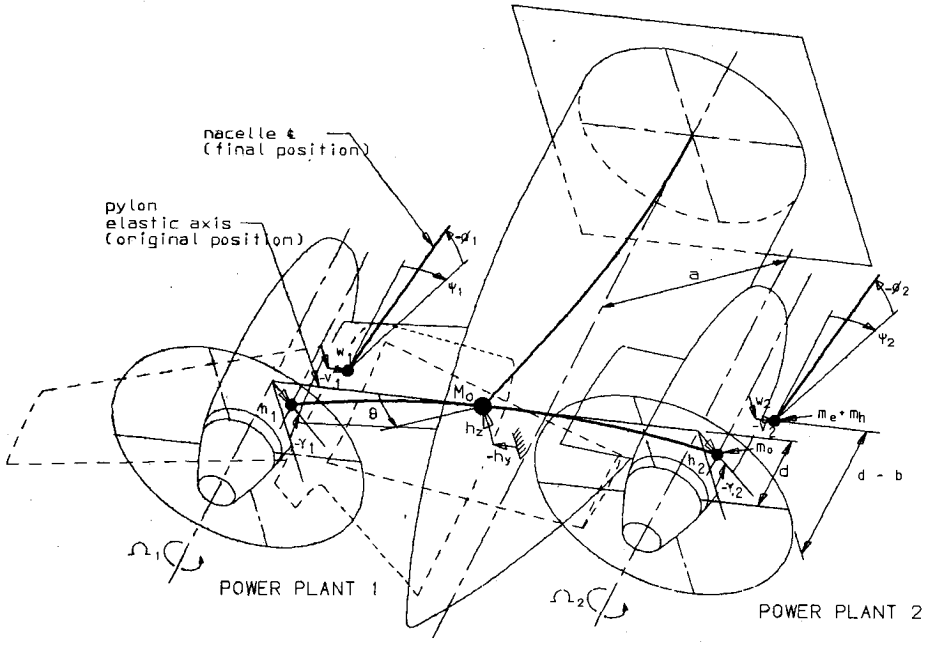

Fig. 1 A 15-degree-of-freedom idealization of the advanced turboprop configuration. The vector of dependent variables is $q = \lfloor \psi_1 v_1 h_y v_2 \psi_2 \vdots \phi_1 \gamma_1 h_1 w_1 h_z \theta\ w_2 h_2 \gamma_2 \phi_2 \rfloor$.

with the previous studies on the influence of the wing flexibility in the whirl-flutter phenomenon, but for this particular aircraft configuration, the backup structure also couples the two propellers, yielding conditions for which the primitive modes of the former are coupled with the whirl modes of the latter in such a way that the disturbing aerodynamic loads are unfavorably summed. In these cases, the presence of the backup structure is detrimental to the system stability.

4) For a certain distance between the pylon elastic axis and the engine-propeller center of mass, the whirl-induced-flutter phenomenon becomes critical.

In the present work, the parametric studies on the whirl-flutter characteristics of advanced turboprops and propfans will be extended in order to allow a better understanding of the whirl-induced-flutter phenomenon identified in Ref. 17.

Aeroelastic Problem Formulation

The 15-deg-of-freedom mathematical model described in Ref. 17 is employed in the present investigation. For the sake of completeness, it is outlined here.

Each engine-propeller installation is modeled as a rigid body, free to move in the lateral, plunge, yaw, and pitch directions. It is not necessary to include the remaining fore-and-aft and roll degrees of freedom of the engine propeller relative to the nacelle. Systematic studies made in the past have indicated that the latter rigid-body degrees of freedom do not play an important role in the whirl-flutter phenomenon and may be omitted.[12,18] According to the same model,[17] the two engines are supported by short pylons cantilevered with the rear fuselage cone, each having two additional degrees of freedom: flatwise bending and torsion about their elastic axes. The remaining three degrees of freedom are represented by the fuselage bending in the vertical and lateral directions and the fuselage torsion about the aircraft centerline (Fig. 1).

The aerodynamic load is assumed to be induced solely by the motion of the two propellers with respect to the undisturbed airstream. Moreover, the flowfield is assumed to be aligned with respect to the fuselage centerline at the wing-fuselage connection to account for the angles of attack induced at the propeller disk by the motion of the entire backup structure. Hence, the two propellers are inertially and aerodynamically coupled by the fuselage degrees of freedom.

The complete theoretical development of the aeroelastic equations is presented in Ref. 17. The aeroelastic system is cast in a set of 15 coupled ordinary differential equations:

$$M\ddot{q} + (G - \mu Q^1)\dot{q} + (K - \mu Q^0)q = 0 \qquad (1)$$

where M is the mass matrix, G the skew-symmetric gyroscopic matrix, and K the diagonal stiffness matrix; Q^1 and Q^0 are the aerodynamic damping (symmetric) and the aerodynamic stiffness matrices, respectively. The generic nature of the latter matrix introduces the eventual instabilities associated with the complex eigenvalues at a nonzero airspeed since all eigenvalues would be pure imaginary numbers if $Q^0 = 0$. The aerodynamic matrices are dependent on geometric parameters describing the propeller position with respect to the pylon elastic axis and the distance between the propeller and the fuselage centerlines. They are also dependent on the aerodynamic influence coefficients, which were defined by Houbolt and Reed.[4] These coefficients, designated in their paper by A_1, A_2, A_3, A_1', and A_2', become a function of only one parameter, the propeller tip speed ratio J, if the aerodynamic properties along the blade span are assumed constant. The vector of dependent variables q is organized in such a way that the dependent variables associated with either the vertical-pitch or the horizontal-yaw displacements of the engines are grouped together; such an arrangement was found to be more natural and, in fact, simplified the coupling among the degrees of freedom in the aeroelastic equations.

The 15 differential equations in the dependent variables are cast in a standard eigenvalue form and then solved for the complex eigenvalues and corresponding eigenvectors. The aeroelastic modes are traced in the Laplace domain both in terms of the propeller tip speed ratio:

$$J/\pi = V/\Omega R$$

and the aerodynamic dimensionless mass ratio

$$\mu = 2N/\bar{m}_\alpha \bar{c}_o$$

where $\bar{m}_\alpha = \rho(\pi c_o^2/4)R/M$ is proportional to the air density ρ (and the aircraft flight altitude); $\bar{c}_o = c_o/R$ is the dimensionless propeller chord, considered constant along the radius R; and N is the number of blades.

Whirl-Flutter Parametric Studies

The most significant geometric parameter to be investigated in a whirl-flutter study is the propeller position with respect to the elastic center of the engine mounting system, which defines the instantaneous apex of the propeller hub precessional motion. The most simplified approach for the whirl-flutter problem considers a two-degree-of-freedom dynamics, in which the elastic center of the engine mounting system relative both to the pitch and yaw motions is fixed. This simplification may be useful when a single plane is employed to support the engine in the nacelle. However, in the more complicated suspension designs, the elastic center of the engine installation is not well defined, and in fact, is continuously changing. Therefore, the concept of an instantaneous apex for the hub precessional motion is more convenient and it is adopted in this work. As the elastic center idealization is no longer useful, any point in the structure may be taken as a geometric reference point. Here, a point at the pylon elastic axis is chosen. The propeller is then positioned at a distance d from the pylon elastic axis aftwards.

Table 1 presents the properties of a hypothetical engine installation to be referred to hereafter as the nominal or reference condition.

Propeller Tip Speed Ratio

Figure 2 depicts the importance of the pylon stiffness on the whirl-flutter stability limits. The case in study is an example for which the critical aeroelastic mode consists of the pylon symmetric bending-torsion out of phase with the fuselage vertical bending. Therefore, the two propellers move in the vertical direction in a symmetric pitching-plunging oscillation while their hubs describe the well-known backward whirl motion with respect to the nacelle. As the corresponding phasor diagram indicates in Fig. 3, the angle between the phasors ψ and ϕ is different from 90 deg. Hence, when the pitch is maximum, the yaw is not necessarily zero. Figure 4 is constructed to help the visualization of the situation described by the pha-

Table 1 Aircraft and engine installation nominal properties

Inertia				Stiffness			
M_o	=	2719 kg		k_y	=	1002 kgf/mm
I_{X_o}	=	1599 kg·m^2		k_z	=	765 kgf/mm
m_o	=	42 kg		k_θ	=	22,000 kgf·m/deg
I_{x_o}	=	5 kg·m^2		k_δ	=	300 kgf/mm
I_{y_o}	=	23 kg·m^2		k_γ	=	2500 kgf·m/deg
m_e	=	420 kg		k_ϕ	=	2740 kgf·m/deg
I_{pe}	=	14.4 kg·m^2		k_ψ	=	4028 kgf·m/deg
I_{te}	=	183 kg·m^2		k_v	=	2770 kgf/mm
m_h	=	100 kg		k_w	=	2770 kgf/mm
I_{ph}	=	21 kg·m^2				
Geometric				Others		
d	=	1.02 m		Ω	=	1700 rpm
b	=	0.260 m		N	=	6
a	=	2.10 m		engine 1	=	$\Omega > 0$
R	=	1.295 m		engine 2	=	$\Omega < 0$
c_o	=	0.254 m		ρ	=	1.225 kg/m^3

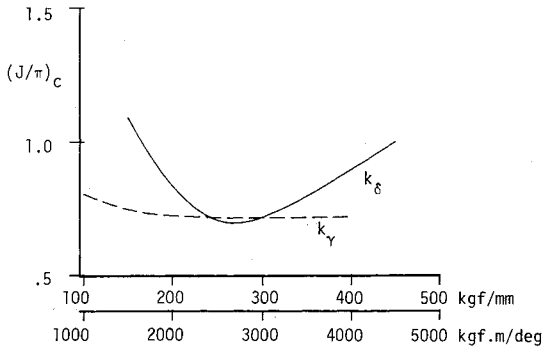

Fig. 2 Pylon stiffness influence on whirl-flutter propeller critical tip speed ratio $(J/\pi)_c$. The nominal configuration is k_γ = 2500 kgf·m/deg and k_δ = 300 kgf/mm. The solid and the dashed curves correspond to parametric variations on k_δ and k_γ, respectively.

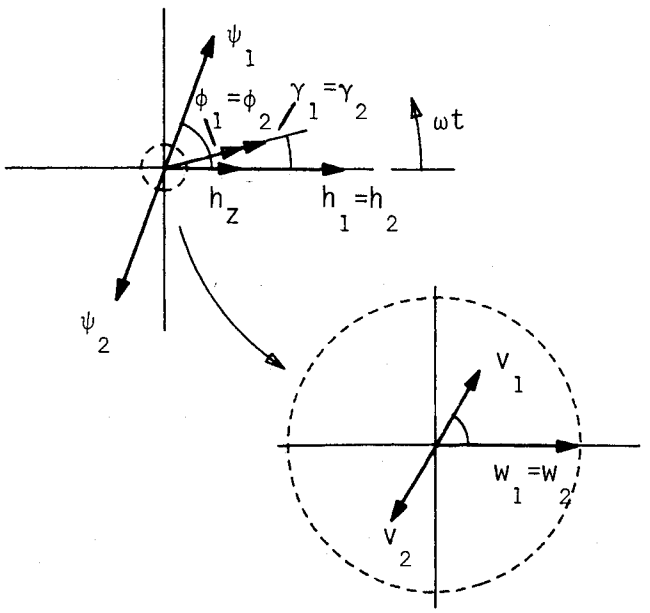

Fig. 3 Phasor diagram for k_γ = 2500 kgf·m/deg and k_δ = 300 kgf/mm at $(J/\pi)_c$ = 0.714: $\psi_1 = -\psi_2$ = 0.68 ∠ 81.1 deg; $\phi_1 = \phi_2$ = 0.39 ∠ 0.15 deg; $\gamma_1 = \gamma_2$ = 0.50 ∠ 0.15 deg; h_z = 0.36 ∠ 0 deg; $h_1 = h_2$ = 1.0 ∠ 0 deg; $v_1 = -v_2$ = 0.023 ∠ 70.7 deg; $w_1 = w_2$ = 0.1 ∠ 0 deg.

sor diagram. The heavy dark spots represent the hub instantaneous positions.

A well-defined minimum in the stability curve around k_δ = 250 kgf/mm is observed in Fig. 2. In a classical whirl-flutter analysis, the presence of this minimum cannot be expected as long as an overall decrease in the stability is expected from the reduction in the system global stiffness. In the present analysis, this minimum is a result of an unfavorable interaction between the aforementioned backup structure natural mode and a propeller whirl mode at a determined frequency. On the other hand, the pylon torsional stiffness is shown in Fig. 2 to be not as sensitive for the system stability for values of k_γ over 2500 kgf·m/deg. The argument that the critical whirl-flutter mode has its major component associated with the pylon bending and not with the pylon torsion, according to Fig. 3, may explain such behavior. Not incidentally, similar results may be obtained with the classical whirl-flutter formulation. Recalling a simple four-degree-of-freedom model, in which only the pitch, yaw, lateral, and vertical displacements of the engine with respect to the nacelle are considered, it is observed that the critical modes change for different ranges of mounting system spring rates, i.e., a critical mostly angular mode (pitch or yaw) becomes stable and a mostly linear mode (lateral or vertical) becomes critical.[18] It is then verified that an increase in the shock mounting system torsional spring rates no longer improves the stability.

In Fig. 5, the engine shock mounting system pitch stiffness is plotted against the critical tip speed ratio. The curve has a minimum around k_ϕ = 2700 kgf·m/deg. Although a similar result may be obtained in a simple two-degree-of-freedom model, the nature of the minimum in the present 15-degree-of-freedom model is quite different in many aspects. In the former case, it is already known that when the pitch and yaw stiffness are equal the trajectory of the hub is circular and the stability reaches its lowest value. The minimum in Fig. 5 is due to the interaction between 1) a backup structure natural mode (pylon symmetric bending-torsion), and 2) an engine mounting system mode (antisymmetric yaw). The two natural modes are coupled by the gyroscopic forces developed by the propeller spin. Figure 5 also demonstrates that, as the pitch stiffness is increased, the frequency of the first mode also increases in the direction of the second mode, which remains almost stationary. At the point where their natural frequencies match, there is a minimum in the value of the critical speed, although the hub trajectory is not circular. This indicates that the coalescence of the two natural frequencies is fundamental for the instability onset. From Table 2 it may be further observed

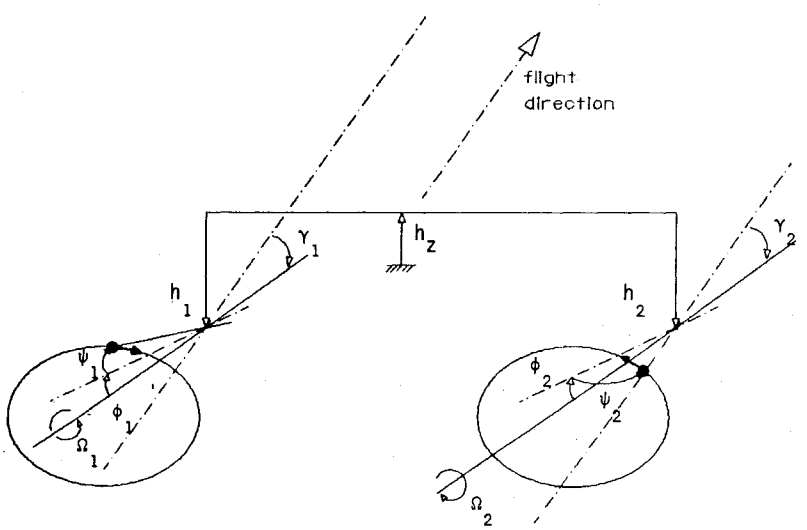

Fig. 4 Schematic representation of the phasor diagram of Fig. 3. The dark spots represent the hub instantaneous positions with respect to the aircraft undisturbed configuration at the whirl-flutter onset. The hub trajectory is described by the curve: $(\phi/|\phi|)^2 + (\psi/|\psi|)^2 - (2\phi\psi/|\phi||\psi|)\cos\beta = 1$, where β is the angle that phasor ψ leads ϕ.

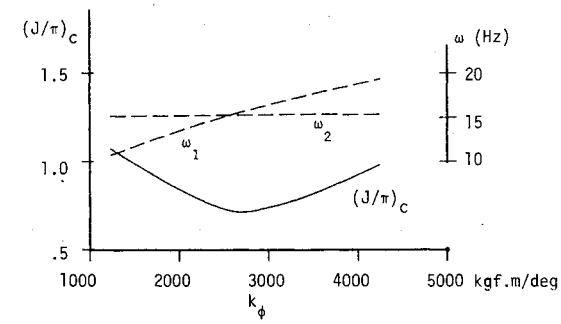

Fig. 5 The quantity k_ϕ vs $(J/\pi)_c$. The dashed lines represent the variation of the natural frequencies of the participating natural modes: 1) pylon symmetric bending-torsion, and 2) engine antisymmetric yaw.

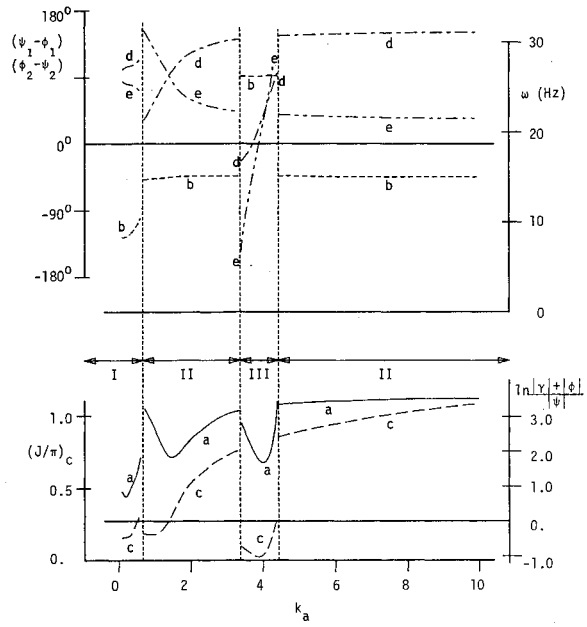

Fig. 6 Parametric study on k_α: a) critical tip speed ratio, $(J/\pi)_c$; b) frequency of the critical eigenmode ω; c) $\ell n[\,(|\phi| + |\gamma|)/|\psi|\,]$; d) and e) relative phase angles between the pitch and yaw displacements for power plants 1 and 2, $(\psi_1 - \phi_1)$ and $(\phi_2 - \psi_2)$ respectively.

that there is an inherent coupling among the components of the same natural modes. In particular, it is verified that the symmetric predominantly backup structure mode 1 has a significant contribution from ϕ, whereas the engine mode 2 consists of an antisymmetric ψ displacement. Since the gyroscopic matrix is skew symmetric, the coupling mechanism of the aeroelastic modes is likely to involve a symmetric and an antisymmetric natural mode. As a result, the modes that were referred to as 1 and 2 have the necessary conditions to be dynamically coupled through their $\phi - \psi$ components as soon as the aerodynamic feedback has been established.

Based on these considerations, the whirl-induced-flutter phenomenon may be interpreted as a generalized form of the classical whirl-flutter problem. The two-degree-of-freedom model reveals that in the most simple case the phenomenon is caused by an interaction between the two uncoupled natural modes of a single engine mounting system, i.e., the pitch and yaw modes. When these modes have the same natural frequencies, the system stability is reduced to its lowest limits.[3-6]

Table 3 presents the critical aeroelastic mode eigenvector at the flutter onset. The reader may note the strong coupling developed between the two natural modes listed in Table 2. It is also noted that the phase difference between the ϕ (engine pitch) and γ (pylon torsion) components of the eigenvector remains zero, indicating that these displacements sum up to yield the total yaw perturbation of the propeller.

Table 2 Critical natural modes $k_a = 1.47$

	Mode 1: 15.2 Hz	Mode 2: 15.7 Hz
ψ_1	—	−1.00
v_1	—	−0.045
h_y	—	—
v_2	—	0.045
ψ_2	—	1.00
ϕ_1	0.375	—
γ_1	0.482	—
h_1	1.00	—
w_1	0.099	—
h_z	0.349	—
θ	—	—
w_2	0.099	—
h_2	1.00	—
γ_2	0.482	—
ϕ_2	0.375	—

Table 3 Critical aeroelastic mode at whirl-flutter onset k_ϕ (kgf·m/deg)/ω(Hz)

	1240/14.6		2740/15.0		4240/15.3	
	Module	Argument, deg	Module	Argument, deg	Module	Argument, deg
ψ_1	1.00	0	0.678	81	0.344	110
v_1	0.014	−34	0.023	71	0.013	85
h_y	—	—	—	—	—	—
v_2	0.014	146	0.023	−109	0.013	−95
ψ_2	1.00	180	0.678	−99	0.344	−70
ϕ_1	0.490	−23	0.392	0	0.503	0
γ_1	0.281	−23	0.501	0	1.00	0
h_1	0.956	−37	1.00	0	0.862	−12
w_1	0.096	−37	0.100	0	0.085	−12
h_z	0.378	−37	0.362	0	0.298	−12
θ	—	—	—	—	—	—
w_2	0.096	−37	0.100	0	0.085	−12
h_2	0.956	−37	1.00	0	0.862	−12
γ_2	0.281	−23	0.501	0	1.00	0
ϕ_2	0.490	−23	0.392	0	0.503	0

A deeper insight in the present multi-degree-of-freedom whirl-flutter analysis is provided by Fig. 6. The curves represent the variation of the characteristic parameters of the system against the ratio between the yaw and pitch stiffnesses, $k_\alpha = k_\psi/k_\phi$, at the whirl-flutter onset. These parameters are, namely, a) the critical tip speed ratio $(J/\pi)_c$; b) the frequency of the critical eigenmode ω; c) the logarithm of the ratio between the engine total pitch amplitude and the engine yaw amplitude $\ell n\,[\,(|\phi| + |\gamma|)/|\psi|\,]$; and d) and e) the relative phase angles between the pitch and yaw displacements for power plants 1 and 2, $(\psi_1 - \phi_1)$ and $(\phi_2 - \psi_2)$, respectively. Each branch of the curves, designated by I, II, and III in Fig. 6, is associated with a different aeroelastic mode, one of which eventually becomes critical in a range of k_α. Although three discontinuities are present in Fig. 6, a closer analysis reveals that the last branch of the curves is a continuation from the second, and so they have been designated by the same Roman character, II. The aeroelastic modes identified by I, II, and III in Fig. 6 evolved from the coupling between two natural modes as follows.

I) First mode (symmetric): engine yaw opposed to fuselage lateral bending; second mode (antisymmetric): engine pitch and pylon torsion opposed to fuselage torsion.

II) First mode (antisymmteric): engine yaw; second mode (symmetric): engine pitch and pylon bending-torsion opposed to fuselage vertical bending.

III) First mode (symmetric): engine yaw-lateral opposed to fuselage lateral bending; second mode (antisymmetric): engine pitch-vertical and pylon bending-torsion opposed to fuselage torsion.

Furthermore, according to the k_α vs $(J/\pi)_c$ curve, each branch has a minimum due to precisely the same reason that explained the minimum in Fig. 2; i.e., in each branch of the curve, at a fixed value of k_α, there is a crossover frequency between the first and the second natural modes described earlier. Moreover, the critical mode II closely resembles the single branch of the classical two-degree-of-freedom model, as long as the minimum around $k_\alpha = 1.5$ corresponds to the circular precessional motion of the propeller hub. The latter conclusion is drawn by observing that, at this particular value of k_α,

$$\ell n\,[\,(|\phi| + |\gamma|)/|\psi|\,] = 0$$

$$\psi_1 - \phi_1 = \phi_2 - \psi_2 = 90 \text{ deg}$$

The same situation would be verified for the two-degree-of-freedom model at $k_\alpha = 1$.

The aircraft configuration studied in the present work has counter-rotating propellers. Therefore, $\psi_1 - \phi_1 > 0$ and $\phi_2 - \psi_2 > 0$ represent backward precessions of the hubs: ψ_1 leads ϕ_1 for engine 1 and ϕ_2 leads ψ_2 for engine 2, whereas $\psi_1 - \phi_1 < 0$ and $\phi_2 - \psi_2 < 0$ represent forward precessions of the hubs. Since in this work it was demonstrated that the whirl-induced-flutter phenomenon is characterized by a dynamics such that a symmetric natural mode containing an engine pitch or yaw component is coupled with an antisymmetric natural mode containing, respectively, a yaw or pitch component, or vice-versa, the resulting aeroelastic mode presents one of the following situations, namely, $\phi_1 = \phi_2$ and $\psi_1 = -\psi_2$, or $\phi_1 = -\phi_2$ and $\psi_1 = \psi_2$. Hence, the relationship

$$(\psi_1 - \phi_1) + (\phi_2 - \psi_2) = \sqrt{180} \text{ deg}$$

is always preserved, which may be checked in curves d and e of Fig. 6 and, in particular, in the phasor diagram of Fig. 3. Incidentally, in a small interval ($3.4 < k_\alpha < 3.8$), the critical condition corresponds to forward whirl modes. In a simplified analysis, both the first and the third branches of the curves in Fig. 6 would not be detected and the stability of the system overestimated.

For the selected configurations in Fig. 6, the root loci of the lower and more interesting aeroelastic modes are constructed in Figs. 7–13. Figures 7, 11, and 13 correspond to the local minima at $k_\alpha = 0.230$, 1.47, and 3.97 of branches I, II, and III of Fig. 6.

Altitude

The altitude enters into the stability problem via the dimensionless aerodynamic mass ratio μ, which multiplies the aerodynamic matrices Q^1 and Q^0. Therefore, when $\mu = 0$, all open-loop poles of the system lie on the imaginary axis at the free-vibration natural frequencies. The system stability at a near-zero value of μ is then a function of the pole departure angles. Since the system characteristic equation is not in Evans's form, the aeroelastic modes evolution with μ does not follow a simple rule. A closer inspection of the system characteristic determinant reveals that μ appears to multiply several terms of the characteristic polynomial under a power 15 or greater. Although it is not an easy task to determine a general rule for the root loci of the aeroelastic modes under this circumstance, some considerations about the stability properties of the system may still be made. A common and dominant feature of the cases analyzed in the present work is the presence of a pair of high-damped modes in the range of 10–15 Hz. One of these modes is symmetric and the other is antisymmetric. They represent a potentially dangerous pair having the discussed necessary conditions to couple with any low-damped mode and generate an eventual instability. In Figs. 14 and 15, the branches associated with two nearby aeroelastic modes are driven onto the unstable region and become critical in a given interval of μ. Therefore, Figs. 14 and 15 depict another important characteristic of the system: they are the root-loci plots for $k_\alpha = 0.605$ and so represent unstable situations at sea

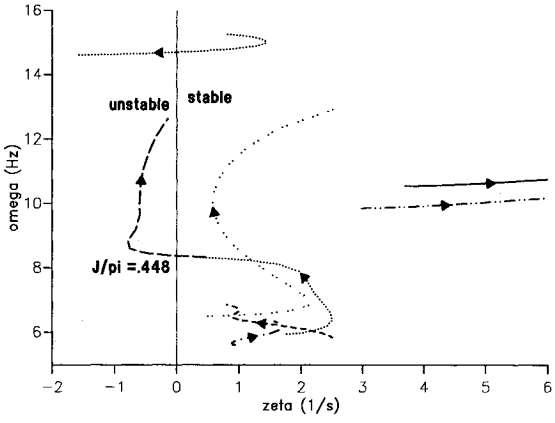

Fig. 7 Root locus vs J/π for $k_\alpha = 0.230$.

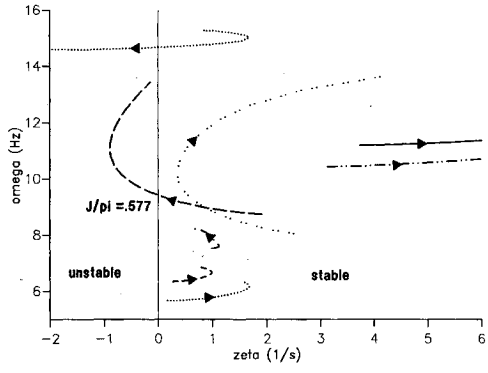

Fig. 8 Root locus vs J/π for $k_\alpha = 0.470$.

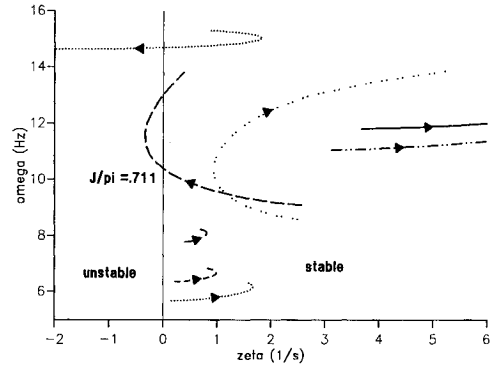

Fig. 9 Root locus vs J/π for $k_\alpha = 0.605$.

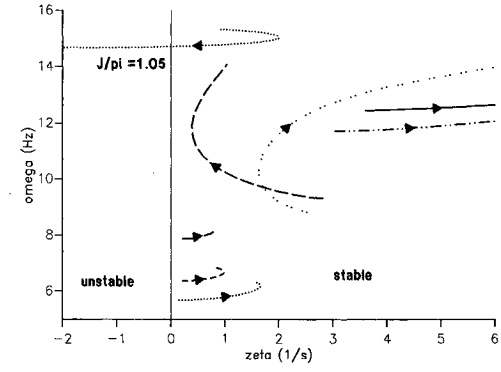

Fig. 10 Root locus vs J/π for $k_\alpha = 0.720$.

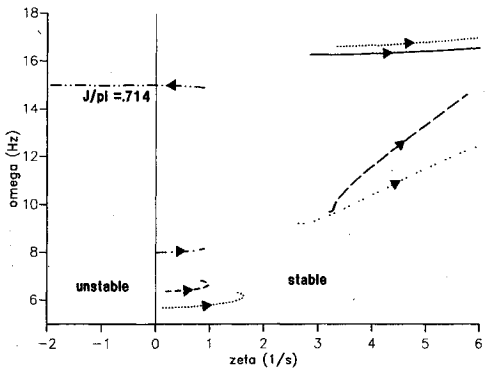

Fig. 11 Root locus vs J/π for $k_\alpha = 1.47$.

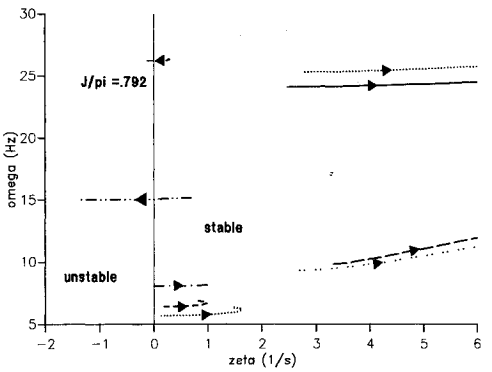

Fig. 12 Root locus vs J/π for $k_\alpha = 3.67$.

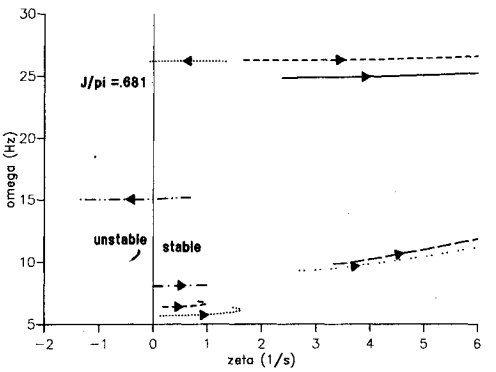

Fig. 13 Root locus vs J/π for $k_\alpha = 3.97$.

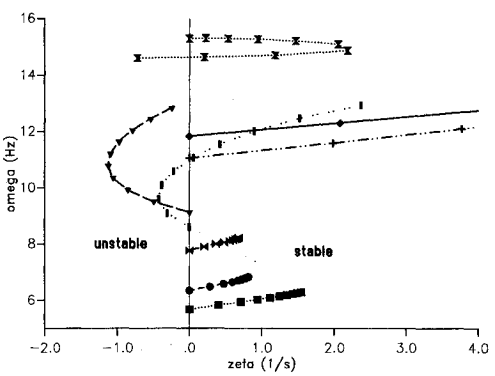

Fig. 14 Root locus vs μ for $J/\pi = 1.22$ and $k_\alpha = 0.605$.

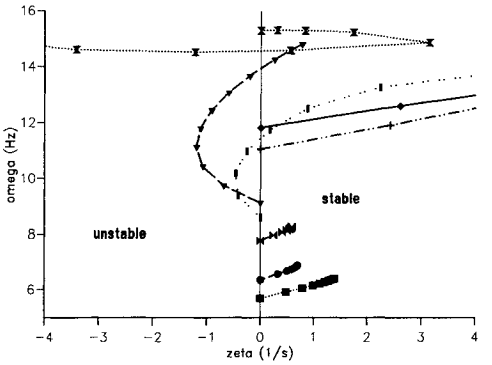

Fig. 15 Root locus vs μ for $J/\pi = 1.52$ and $k_\alpha = 0.605$.

level, at $J/\pi = 1.22$ and 1.52, respectively. The first root loci presents two unstable roots at sea level, whereas the second only one. In the former case, the mounting system viscous damping may help to stabilize the roots at a low value of μ, but the same cannot be expected in the latter due to the large negative damping achieved by the system at the sea-level condition. As a conclusion, an increase in the altitude may or may not be detrimental to the system stability.

Conclusions

One of the most important features of the system subjected to the critical conditions determined by whirl-induced flutter is a large stability margin based on the fact that for the majority of situations the backup structure acts as a dynamic damper, absorbing energy from the engine mounting system. Therefore, it is feasible to assume the backup structure as an integrated part of the design of the engine suspension and, while keeping the whirl-flutter stability, to improve the transmissibility characteristics of the vibration insulators. The engine shock mounts and the backup structure work as springs in series, for which only the former has good damping properties. Hence, if the two idealized springs have equivalent stiffnesses, it is likely that the engine mounting system becomes less efficient as a vibration insulator. In summary, an optimal design problem is posed for which a careful analysis is obviously rewarding. The multiplicity of maxima and minima that characterizes the behavior of the stability curves suggests that this technique may be widely used for a particular engine installation to achieve better results. However, the present work emphasizes that it is not an easy task to develop a safe engine suspension for a modern turboprop or propfan configuration. The gyroscopic forces generated by the two rear-fuselage-mounted propellers are responsible for an interaction between the familiar propeller-nacelle whirl modes and the structure natural modes. An extensive parametric investigation showed the following.

1) The onset of instability may be associated with a mode of the backup structure. This phenomenon was called whirl induced flutter to differentiate it from the classical whirl flutter for which the critical modes are derived solely from the motion of the engine with respect to the nacelle.

2) The whirl-induced-flutter phenomenon may be regarded as a generalization of the classical two-degree-of-freedom phenomenon.

3) The properties of symmetry (and antisymmetry) inherent to the turboprop or propfan power plant installation not only help to understand on physical grounds the critical conditions developed in the mathematical model, but also provide to the analyst a systematic procedure to select the most important natural modes of the structure to be retained in the whirl-flutter investigation.

References

[1]Taylor, E. S., and Browne, K. A., "Vibration Isolation of Aircraft Power Plants," *Journal of the Aeronautical Sciences*, Vol. 6, No. 12, 1938, pp. 43–49.

[2]Abbott, F. T., Jr., Kelly, H. N., and Hampton, K. D., "Investigation of Propeller Power-Plant Autoprecession Boundaries for a Dynamic Aeroelastic Model of a Four-Engine Turboprop Transport Airplane," NASA TN-D-1806, Aug. 1963.

[3]Reed, W. H., III, and Bland, S. R., "An Analytical Treatment of Aircraft Precession Instability," NASA TN-D-659, Jan. 1961.

[4]Houbolt, J. C., and Reed, W. H., III, "Propeller Nacelle Whirl-Flutter," *Journal of Aerospace Sciences,* Vol. 29, No. 3, 1962, pp. 333–346.

[5]Sewall, J. L., "An Analytical Trend Study of Propeller Whirl Instability," NASA TN-D-996, April 1963.

[6]Bland, S. R., and Bennett, R. M., "Wind Tunnel Measurement of Propeller Whirl-Flutter Speeds and Static Stability Derivatives and Comparison with Theory," NASA TN-D-1807, Aug. 1963.

[7]Ribner, H. S., "Propeller in Yaw," NACA Rept. 820, 1945.

[8]Zwaan, R. J., and Bergh, H., "Propeller-Nacelle Flutter of the Lockheed Electra Aircraft," National Aerospace Laboratory, Amsterdam, The Netherlands, Rept. F-288, Feb. 1962.

[9]Bennett, R. M., and Bland, S. R., *Experimental and Analytical Investigation of Propeller Whirl-Flutter of a Power Plant on a Flexible Wing,* NASA TN-D-2399, Aug. 1964.

[10]Head, A. L., Jr., "A Review of the Structural Dynamic Characteristics of the XC-142A Aircraft," *Proceedings of the CAL/TRECOM Symposium, Dynamic Load Problems Associated with Helicopters and V/STOL Aircraft,* Vol. 2, 1963.

[11]Ravera, R. J., "Effects of Steady State Blade Angle of Attack on Propeller Whirl-Flutter," Grumman Aircraft Engineering Corp., Rept. ADR 06-01-63.1, 1963.

[12]Baker, K. E., Smith, R., and Toulson, K. W., "Notes on Propeller Whirl-Flutter," *Canadian Aeronautics and Space Journal,* Vol. 11, No. 8, 1965, pp. 305–313.

[13]Richardson, J. R., and Naylor, H. F. W., "Whirl Flutter of Propellers with Hinged Blades," Directorate Engineering Research, Defense Board, Toronto, Canada, Rept. 24, March 1962.

[14]Reed, W. H., III, and Bennett, R. M., "Propeller Whirl-Flutter Considerations for V/STOL Aircraft," *Proceedings of the CAL/TRECOM Symposium, Dynamic Load Problems Associated with Helicopters and V/STOL Aircraft,* Vol. 3, 1963.

[15]Richardson, J. R., McKillop, J. A., Naylor, H. F. W., and Blander, P. A., "Whirl Flutter of Propellers with Flexible Twisted Blades," Directorate Engineering Research Defense Board, Toronto, Canada, Rept. 43, Jan. 1963.

[16]Johnson, W., "Analytical Modeling Requirements for Tilting Proprotor Aircraft Dynamics," NASA TN-D-8013, July 1975.

[17]Nitzsche, F., "Whirl-Flutter Investigation on an Advanced Turboprop Configuration," *Journal of Aircraft,* Vol. 26, No. 10, 1989, pp. 939–946.

[18]Resende, H. B., "Estudos na Análise de Whirl-Flutter," M.S. Thesis, Instituto Tecnológico de Aeronáutica, CTA, São José dos Campos, Brazil, 1987.